Supplemental Material

Journal of Applied Meteorology and Climatology
Future Change in the Contribution of Riming and Depositional Growth to the Surface Solid Precipitation in Hokkaido, Japan
https://doi.org/10.1175/JAMC-D-23-0226.1

Supporting information of "Future change in the contribution of riming and depositional growth to the surface solid precipitation in Hokkaido, Japan"

Yousuke Sato[a,*], Moeka Kamada[b], Akihiro Hashimoto[c], and Masaru Inatsu[a]

[a] *Faculty of Science, Hokkaido University, Sapporo, Hokkaido, Japan*

[b] *Graduate School of Science, Hokkaido University, Sapporo, Hokkaido, Japan*

[c] *Meteorological Research Institute, Tsukuba, Ibaraki, Japan*

Contents of this file

S1. Brief description of the process tracking model (PTM)

PTM is one of the novel methods used in this study, and it was originally developed by Hashimoto et al. (2020) to examine the mass fraction of the depositional growth and riming processes relative to the mass of cloud hydrometeors. PTM predicts the mass of the hydrometeor produced by the riming process and depositional growth (shown in Table S1) for each solid hydrometeor category considered in bulk microphysical models. For the two moment bulk microphysical schemes used in this study (Seiki and Nakajima 2014), which predict the mixing ratio and number concentration of cloud ice (q_i and N_i), snow (q_s and N_s), and graupel (q_g and N_g) as the categories for the solid hydrometeor, PTM predicts the mixing ratio of the seven categories shown in Table S1 ($q_{(i,s,g),dep0}$, $q_{(i,s,g),dep4}$, $q_{(i,s,g),dep10}$, $q_{(i,s,g),dep14}$, $q_{(i,s,g),dep20}$, $q_{(i,s,g),dep36}$, and $q_{(i,s,g),rim}$) for the category of each solid hydrometeor (i.e., cloud ice, snow, and graupel). Thus, 21 prognostic variables were calculated in addition to the original prognostic variables. According to Nakaya (1954), the habit of the snowfall particles generated by each process is roughly associated with the categories shown in Table S1.

The governing equation of $q_{(i,s,g),p}$ in SCALE is described as follows based on Nishizawa et al. (2021):

$$\frac{\partial(\rho q_{x,p})}{\partial t} + \nabla \cdot (\rho q_{x,p} u) = \left(\frac{\partial(\rho q_{x,p})}{\partial t}\right)_{phys} + \left(\frac{\partial(\rho q_{x,p})}{\partial t}\right)_{MP}, \qquad \text{(S1)}$$

where ρ represents density, u represents the wind vector, x corresponds to the solid precipitation category (i.e., i, s, and g), and p represents categories shown in Table S1 (e.g., Dep0, Dep4, Rim and so on). The second term of the left hand side shows the effects of advection; the second term in the right hand side shows the production and the loss term by microphysical processes (MPs), including sedimentation; and the first term of the right hand side shows the production and loss term by other physical processes, such as turbulence and diffusion. According to Hashimoto et al. (2020), the production and loss term by MPs are described by eqs. S2 and S3.

$$\left(\frac{\partial(\rho q_{x,dep\#})}{\partial t}\right)_{MP} = \left(\frac{\partial(\rho q_{x,dep\#})}{\partial t}\right)_{dep\#} + \sum_{y=i,s,g(y\neq x)} \left[\frac{q_{x,dep\#}}{q_x}\left(\frac{\partial(\rho q_x)}{\partial t}\right)_{x\to y} + \frac{q_{y,dep\#}}{q_y}\left(\frac{\partial(\rho q_y)}{\partial t}\right)_{x\to y}\right] \qquad \text{(S2)}$$

$$\left(\frac{\partial(\rho q_{x,rim})}{\partial t}\right)_{MP} = \left(\frac{\partial(\rho q_{x,rim})}{\partial t}\right)_{rim} + \sum_{y=i,s,g(y\neq x)} \left[\frac{q_{x,rim}}{q_x}\left(\frac{\partial(\rho q_x)}{\partial t}\right)_{x\to y} + \frac{q_{y,rim}}{q_y}\left(\frac{\partial(\rho q_y)}{\partial t}\right)_{x\to y}\right] \qquad \text{(S3)}$$

where # represents temperature range of depositional growth in Table S1 (i.e., 0, 4, 10, 14, 20, 36, other) and *x* and *y* indicate the categories of solid precipitation (i.e., *i*, *s*, and *g*). The first term of the right hand side of eq. S2 is the production and loss term of $q_{x,dep\#}$ by depositional growth (eq. S4) and that of eq. S3 is the production and loss term of $q_{x,rim}$ by riming. The second term in eqs. S2 and S3 is the production and loss term by accretion (eqs. S5–S7).

$$\left(\frac{\partial(\rho q_{x,dep\#})}{\partial t}\right)_{dep\#} = P_{x,dep\#} \quad \text{(S4)}$$

$$\left(\frac{\partial(\rho q_{i,rim})}{\partial t}\right)_{rim} = P_{i,iacw} \quad \text{(S5)}$$

$$\left(\frac{\partial(\rho q_{s,rim})}{\partial t}\right)_{rim} = P_{s,sacw} \quad \text{(S6)}$$

$$\left(\frac{\partial(\rho q_{s,rim})}{\partial t}\right)_{rim} = P_{g,iacw} + P_{g,sacw} + P_{gacw} \quad \text{(S7)}$$

where $P_{x,dep\#}$ represents the increase of the density weighted mixing ratio of category *x* by depositional growth under the temperature range # shown in Table S1; $P_{i,iacw}$ and $P_{g,sacw}$ represent the change in the mixing ratio of cloud ice and graupel by the accretion of cloud droplets by cloud ice; $P_{s,sacw}$ and $P_{g,sacw}$ represent the change in the density weighted mixing ratio of cloud ice and graupel by the accretion of cloud droplets by snow; and P_{gacw} represents the change in the density weighted mixing ratio by the accretion of cloud droplets by graupel.

The large mass fraction of some PTM categories does not directly correspond to the habit of the ice crystal. In nature, solid precipitation particles have various habits that do not necessarily correspond to typical habits but are often a mixture of habits. PTM represents the mixture of habits by the mass fraction of depositional growth and riming. Thus, the large mass fraction of each category does not directly correspond to the habit of the solid precipitation particles. To identify this, we refer to the mass fraction for each category of PTM according to the depositional growth of the habit in Table S1 or riming, with the first capital letter for each habit presented in the body of the manuscript.

Table S1. Prognostic variables of PTM for each solid hydrometeor category (i.e., cloud ice, snow, and graupel) and its corresponding habits (Nakaya 1954). T and S_i represent temperature in °C and supersaturation over ice in %, respectively.

	Deposition						Riming
T (°C)	$-4 < T < 0$	$-10 < T < -4$	$-20 < T < -10$[*1]	$-17 < T < -14$[*1]	$-20 < T < -36$	$T < -36$	
S_i (%)				$S_i > 7$[*1]			
Habit (Nakaya 1954)	Irregular needle	Needle/ Columnar	Plate	Dendrite	Columnar	Other	Rimed particle
Notation	Dep0	Dep4	Dep10	Dep14	Dep20	Dep36	Rim

*1: Habit corresponds to Plate (Dep10) when $-17 < T < -14$ °C and $S_i < 7$ % and when $-20 < T < -17$ °C or $-14 < T < -10$ °C regardless of S_i (Dep10).

S2. Discussion about the representativeness of the target period

In this study, the simulations for Dec. 2020 to Feb. 2021 (2020/21 winter, DJF) were conducted as the present day (PD) experiment. The representativeness of the target period should be confirmed because the bias in PD can result in biased knowledge about future change. The representativeness was confirmed by analyzing the temperature at 850 hPa, which is near the cloud layer levels in the target period. For the analyses, temperature data from the Japanese 55-year Reanalysis data (JRA-55: Harada et al. 2016; Kobayashi et al. 2015) from 1960 to 2023 (63 years) were used.

Based on the analysis of air temperature averaged across the domain encompassing Hokkaido (i.e., 137.5-147.5E, 40-46.25N), the DJF-mean air temperature at 850 hPa was only 0.17 K colder than the recent 63-year average temperature (Fig. S1). The histogram of 6-hourly temperature data is closest to the climatological histogram for the analyzed 63 years, as indicated by the discrete Kullback–Leibler divergence diagnosis (Fig. S2). This suggests that the region around Hokkaido experienced temperatures in 2020/21 winter that closely followed the climatological probability. Moreover, principal component (PC) analysis for sea-level pressures around Japan (127.5-157.5E, 27.5-55N) revealed that the DJF-mean PC1 in 2020/21 had a value of only 0.08, which was approximately 1/3 of the standard deviation

for the recent 63 years. Consequently, the 2020/21 winter period is considered a typical winter in terms of the direct influence of the background field on water vapor supply to the atmosphere through the lake effect or extratropical cyclone passages.

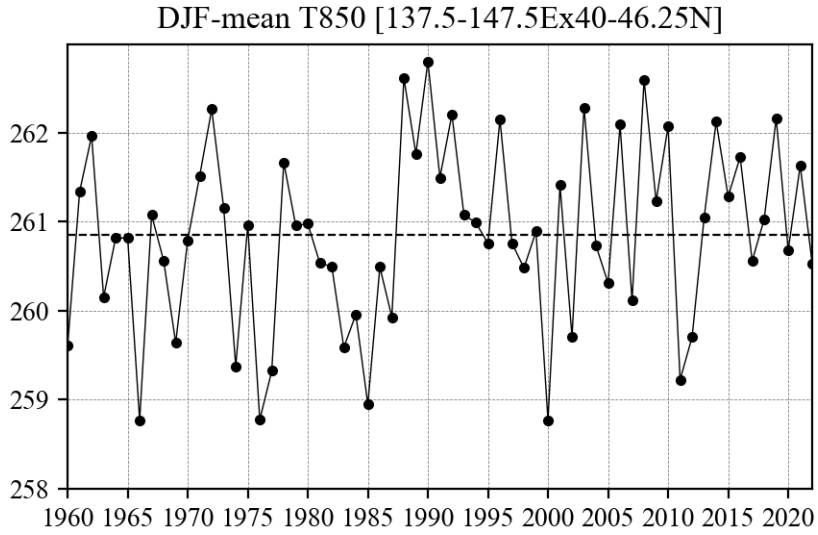

Fig. S1: DJF-mean air temperatures in units of K at 850 hPa averaged over the domain (137.5-147.5E, 40-46.25N) from 1960/61 to 2022/23 winter (December, January, and February: DJF). The dotted line indicates the 63-year average.

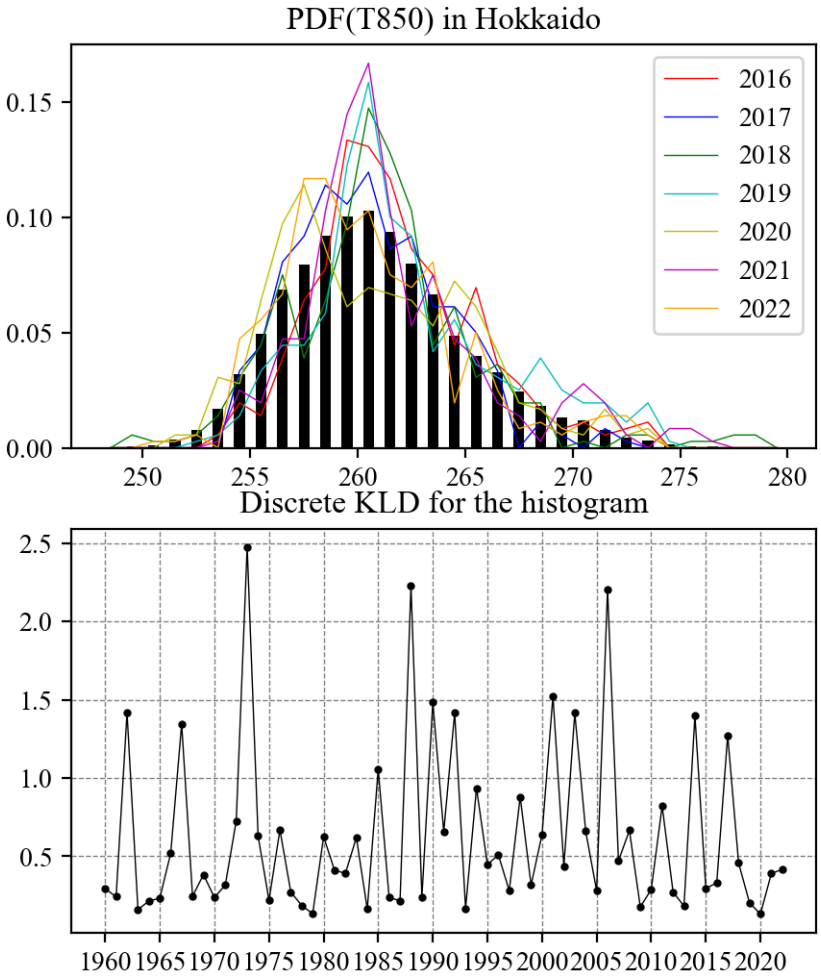

Fig. S2: (top) The probability density function (PDF; K^{-1}) of 850-hPa temperatures (K in horizontal axis) in the Hokkaido domain for each winter from 2016/17 to 2022/23 based on the JRA55 reanalysis data with a 6-hourly data sampling interval. The lines are colored according to the legend, and the values are superimposed with the climatological PDF in the bar graph. The bin size is 1 K. (bottom) The discrete Kullback–Leibler divergence, defined as $\sum p_i \log(p_i/q_i)$, to diagnose the each-winter PDF q similarity to the climatological p.

S3. Figures S3-S5

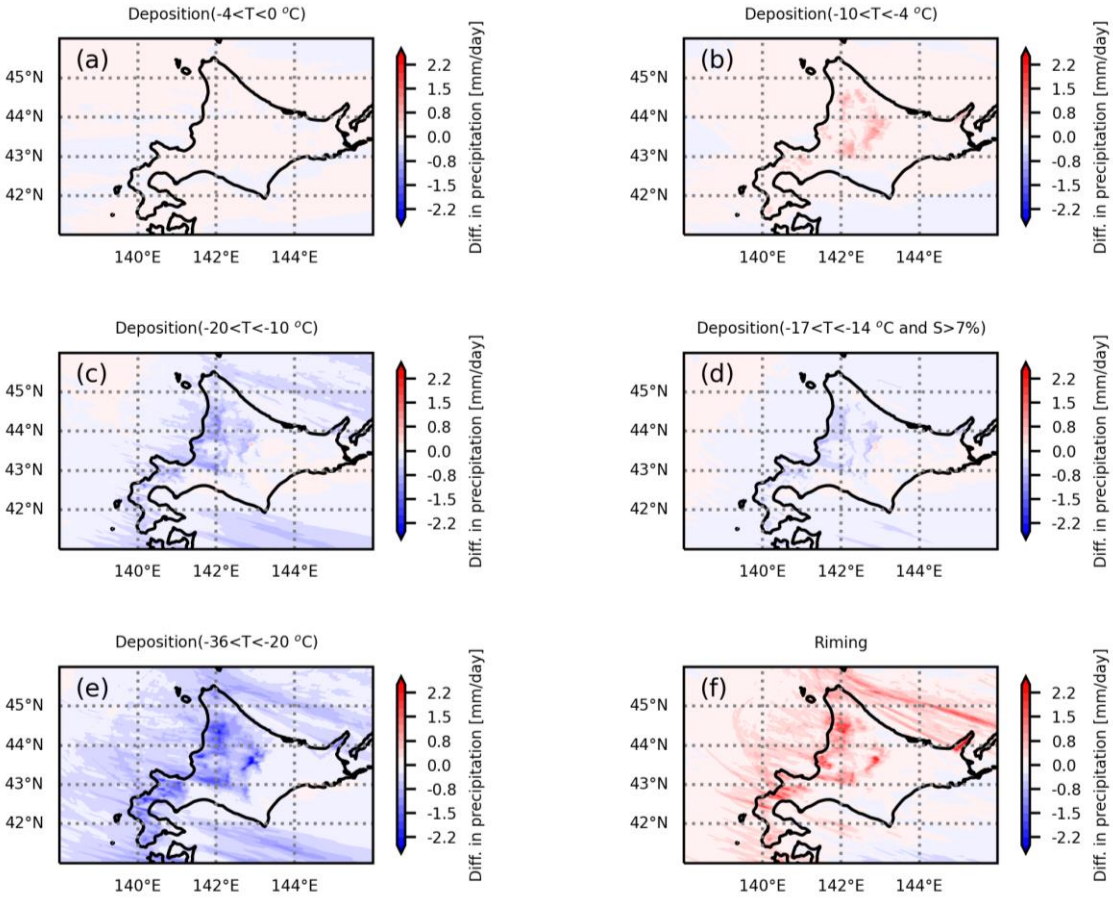

Fig. S3. Geographical distribution of the difference in the mass fraction to the surface precipitation by the depositional growth of (a) –4 °C < T < 0 °C (Irregular Needle), (b) –10 °C < T < –4 °C (Needle/Columnar), (c) –20 °C < T < –10 °C (Plate), (d) –17 °C < T < –14 °C and S_i > 7 % (Dendrite), (e) –36 °C < T < –20 °C (Columnar), and (f) the riming process (Riming) between 4K and PD for December. The difference was defined as the results of 4K minus those of PD.

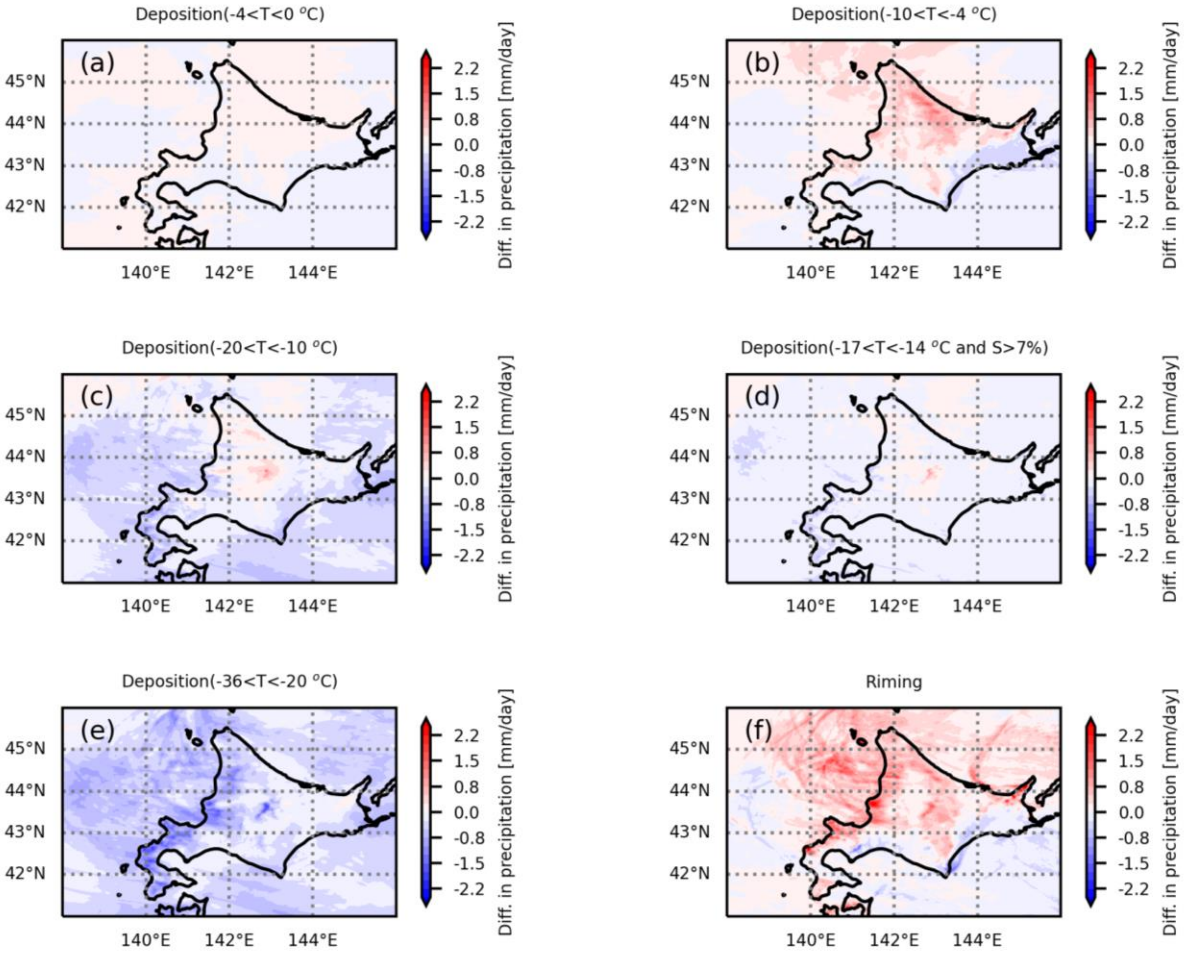

Fig. S4. Same as in Fig. S3 but for January.

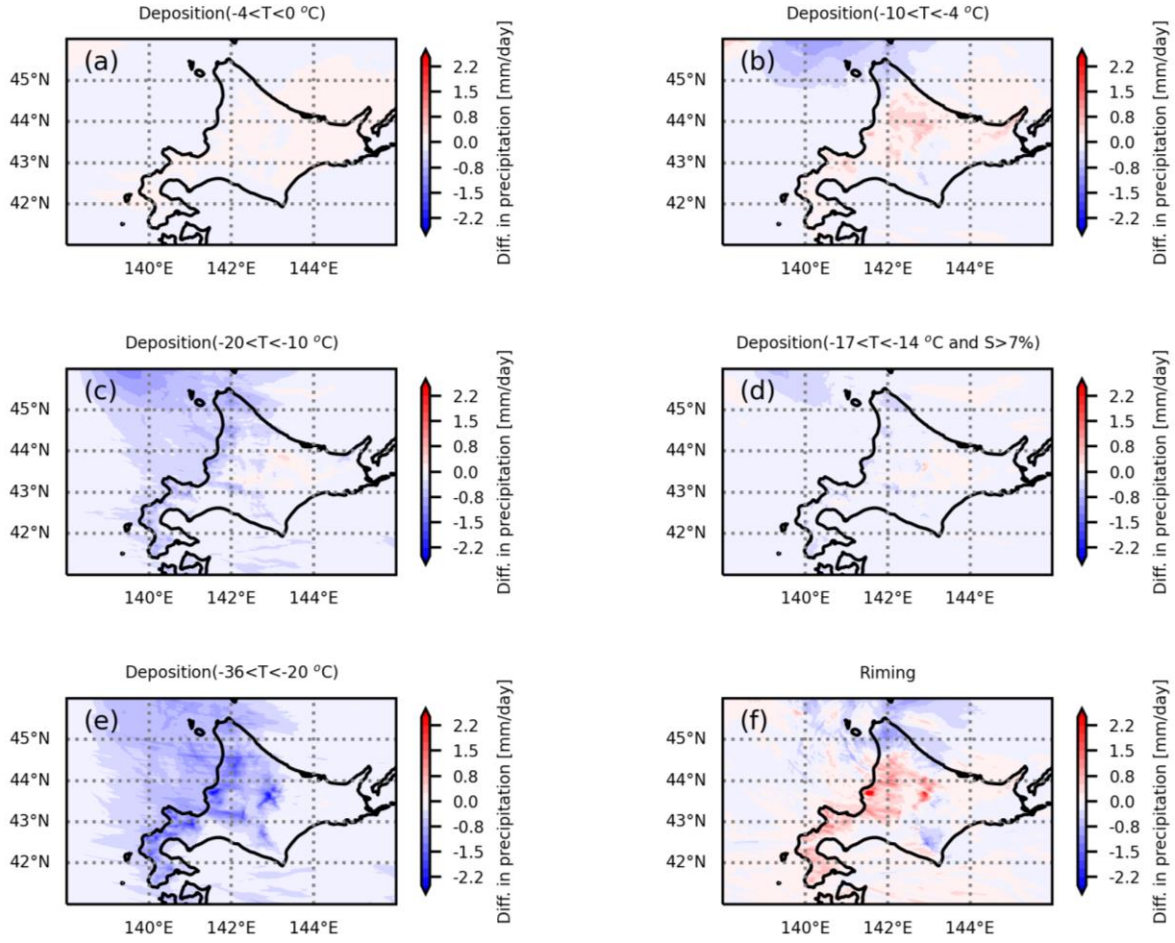

Fig. S5 Same as in Fig. S3 but for February.

References

Harada, Y., H. Kamahori, C. Kobayashi, H. Endo, S. Kobayashi, and Y. Ota, 2016: The JRA-55 Reanalysis: Representation of atmospheric circulation and climate variability. *J. Meteorol. Soc. Jpn.*, **94**, 269–302, https://doi.org/10.2151/jmsj. 2016-015 J-STAGE.

Hashimoto, A., H. Motoyoshi, N. Orikasa, and R. Misumi, 2020: Process-tracking scheme based on bulk microphysics to diagnose the features of snow particles. *SOLA*, **16**, 51–56, https://doi.org/10.2151/sola.2020-009.

Kobayashi, S., and Coauthors, 2015: The JRA-55 reanalysis: general specifications and basic characteristics. *J. Meteorol. Soc. Jpn. Ser. II*, **93**, 5–48, https://doi.org/10.2151/jmsj.2015-001.

Nakaya, U., 1954: *Snow crystals, natural and artificial*. Harvard University Press, 510 pp.

Nishizawa, S., H. Tomita, and T. SCALE, 2021: Detailed formulation of SCALE-RM. 136. https://scale.riken.jp/archives/scale_rm_description-5.4.5.pdf (accessed on Mar. 13, 2024)

Seiki, T., and T. Nakajima, 2014: Aerosol effects of the condensation process on a convective cloud simulation. *J. Atmos. Sci.*, **71**, 833–853, https://doi.org/10.1175/JAS-D-12-0195.1.